MAGNETOHYDRODYNAMICS Vol. 40 (2004), No. 1, pp. 3–21

INDUCTION MECHANISMS IN VON KÁRMÁN SWIRLING FLOWS OF LIQUID GALLIUM

M. Bourgoin[1], *R. Volk*[1], *P. Frick*[2],
S. Khripchenko[2], *Ph. Odier*[1], *J.-F. Pinton*[1]

[1] *Laboratoire de Physique, ENS, 46 allée d'Italie, F-69007, Lyon, France*
[2] *Institute of Continuous Media Mechanics, Korolyov 1, 614061 Perm, Russia*

Using *in situ* magnetic field measurements, we study the induction mechanisms in a swirling flow of liquid Gallium generated inside a cylinder, in the gap between two coaxial rotating discs. The von Kármán flow generated in this manner has both helicity and differential rotation. Magnetic Reynolds numbers Rm up to 7 (based on the disc rim speed) are generated. We study the magnetic induction when an external field is applied successively along the axis, in the azimuthal direction or tranverse to the axis of rotation. In the first two cases, both the flow and the magnetic field are axisymmetric, and an effective mechanism of conversion from poloidal to toroidal field exists but, in agreement with Cowling's theorem, no reciprocal mechanism can be identified. When the applied magnetic field is transverse to the flow, the axial symmetry is broken and several non-axysimmetric mechanisms can generate an axial field from the applied transverse one: a linear (in Rm) induction by the radial gradients of the poloidal flow; a quadratic (in Rm), Parker-like, induction by the flow helicity and an effect entirely due to the discontinuity of electrical conductivity at the boundary of the flow. In all of our observations, the mean induction can be explained using the topology of the von Kármán mean flow, *i.e.* without having to invoke the effects of turbulent fluctuations.

1. Introduction. A complex flow of an electrically conducting fluid can under some conditions generate a large-scale magnetic field [1–3]. This phenomenon is called the magnetohydrodynamic (MHD) dynamo. The MHD dynamo is thought to be responsible for the initiation and maintenance of magnetic fields in space bodies, e.g., the Sun and the Earth [1, 4]. Following the current understanding, the dynamo process in space bodies is based on the interactions between poloidal and toroidal modes of the magnetic field. For a planet, having a dipolar magnetic field with an axis parallel to its axis of rotation, a typical dynamo cycle should include two main mechanisms: the first one must generate a toroidal magnetic field from a given poloidal one and the second one should be responsible for the generation of a poloidal field from a given toroidal field. The first process is easily achieved by differential rotation, which usually takes place in astrophysical flows (the lines of poloidal magnetic field are spooled around the axis of rotation). The second element of the dynamo cycle is more subtle: it cannot be achieved by a laminar axisymmetric flow (Cowling's theorem), but it can exist if the axial symmetry is broken at smaller scales, particularly, if the subscale motion is helical. This process is at the heart of the Roberts dynamo [5], which underlies the Karlsruhe experiment [6]. Self-generation of a non-stationary dynamo magnetic field is also possible from a single helical flow, as analytically proposed by Ponomarenko [7] and experimentally demonstrated in the Riga experiment [8].

We consider here the class of von Kármán flows, generated inside a cylinder by the rotation of one or two coaxial discs. Laminar flows of this kind have been shown to be able to generate a dynamo [9], in particular, when driven by two counter-rotating discs [10]. They are actively studied by several groups around

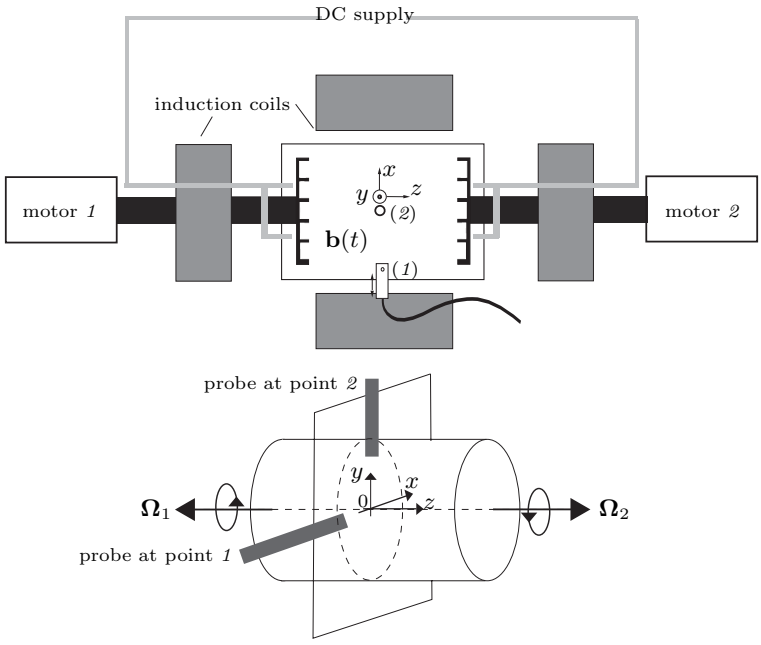

Fig. 1. Experimental setup: sketch of the experiment with magnetic coils and probe position. The upper figure is the top view of the experiment.

the world [11]. The main property of these flows is that their velocity field has both differential rotation and helicity. The aim of this paper is to describe in details the induction mechanisms in this geometry, as can be observed by the response to an externally applied magnetic field. The magnetic Reynolds number Rm which can be achieved in our experiments is less than ten, so that dynamo action cannot be directly observed. We consider the case of applied fields $\mathbf{B}^{\mathrm{A}}$ that can either have the axisymmetry of the von Kármán mean flows (when $\mathbf{B}^{\mathrm{A}}$ is axial or azimuthal) or brake it, as when $\mathbf{B}^{\mathrm{A}}$ is perpendicular to the axis of the cylinder. The generation by differential rotation of a toroidal field from an applied axial field has been previously reported [12], and will be discussed in greater details in section 4 of this paper, where we also report the global measurements of the potential difference across the length of the cylinder. In this geometry, if one searches for a dipolar dynamo with a magnetic dipole parallel to the axis of rotation, one needs a mechanism to generate an axial field from an applied toroidal one. Because of Cowling's theorem, this possibility relies entirely on the turbulent fluctuations in the flow, through eventual small scale α or β effects [14, 15]. We study in detail the flow response to an applied azimuthal field in section 5, and conclude that we do not observe any evidence of such effects up to the limited values of the magnetic Reynolds number achieved here. Finally, we consider in section 6 the case of an applied field perpendicular to the axis of the cylinder. In this case, the axisymmetry of the induction is broken. An axial magnetic field is induced from the transverse applied field, which is not axisymmetric and which has very different contributions according the location. When the helical flow is produced by the rotation of one disc, an axial component linear in Rm is generated at points located on the meridional plane parallel to the applied field (by the differential axial pumping of the flow). In the perpendicular plane, the axial induced field is quadratic in Rm (it is the macroscopic α or Parker effect [16, 17]).

When both discs are counter-rotating at the same speed, we show that the main contribution to the induction in the mid-plane is linear in Rm and it is due to the boundary conditions at the lateral walls of the flow. This effect, though resulting from simple electromagnetism arguments, has not been reported previously or even considered in the analysis of induction in this flow geometry. The paper ends with a discussion of the relevance of our observations in regards to the induction and dynamo self-generation in von Kármán flows.

2. Experimental setup.

2.1. Flow. Our experiments are carried out in the setup sketched in Fig. 1. The flow is driven by the rotation of one or two discs inside a stainless steel cylindrical vessel filled with liquid Gallium. The cylinder radius R is 97 mm and its length is 323 mm. The discs have a diameter equal to 165 mm and are fitted a set of 8 blades with height 10 mm. They are separated by a distance $H = 203$ mm. The discs are driven by two 11 kW AC-motors, which provide a constant rotation rate in the interval 0.5–25 Hz with a stability of about 0.1%. The system is cooled by a set of coils located behind the driving discs; the experiments are made with the flow kept at a temperature in an interval between 42°C and 48°C. The fluid is liquid Gallium (density $\rho = 6.09 \times 10^3$ kgm^{-3}), chosen for its high electrical conductivity ($\sigma = 3.68 \times 10^6$ ohm^{-1}m^{-1}). Its kinematic viscosity is $\nu = 3.1 \times 10^{-7}$ m^{2}s^{-1}. The integral kinematic and magnetic Reynolds numbers of the flow are defined as $\mathrm{Re} = 2\pi R^2\Omega/\nu$ and $\mathrm{Rm} = 2\pi\mu_0\sigma R^2\Omega$. Values of Rm up to 7 are achieved, with corresponding Re in excess of 10^6. Note that, as in all liquid metals, the magnetic Prandtl number $\mathrm{Pm} = \mu_0\sigma\nu$ is very small (of the order of 10^{-6}). Thus, the flow is strongly turbulent even at the moderate values of Rm reached in our experiment.

This setup allows us to study the so-called von Kármán flow between two discs rotating with angular velocities fixed at Ω_1 and Ω_2 (in Hz, *i.e.* revolutions per second) – conventional positive directions of rotation are indicated in Fig. 1. For a given vessel, discs and liquid, these two velocities completely define the flow in the cylinder. When only one disc rotates, the flow velocity involves a toroidal component and a single poloidal cell due to the pumping action of the disc – Fig. 2*a*. When the two discs counter-rotate, two such cells develop in each half of the flow vessel, as shown in Fig. 2*b*. Note that the expression 'counter-rotating discs' implies $\Omega_1 = \Omega_2$, unless otherwise stated. The control parameters of the flow can be alternatively specified by the set (Δ, Σ), where $\Delta = \Omega_2 - \Omega_1$ and $\Sigma = \Omega_1 + \Omega_2$ – see Fig. 2*c*. The first one, Δ, defines the contribution of each

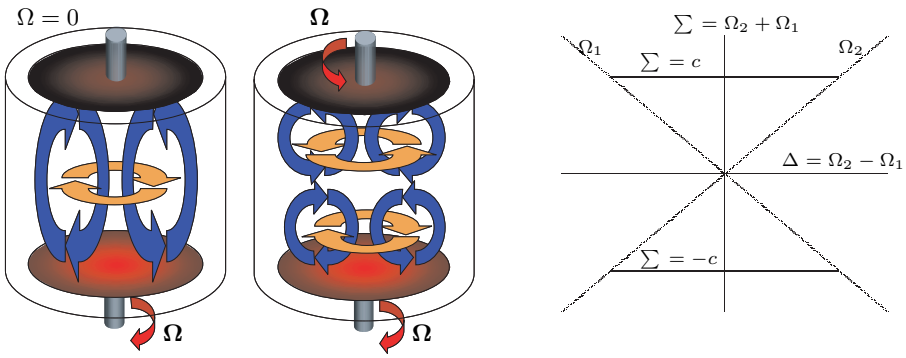

Fig. 2. (*a*), (*b*) Sketch of the mean flow geometry; (*c*) parameter plan.

disc: $\Delta = 0$ implies that two discs counter-rotate at the same velocity; $\Delta = \pm\Sigma$ corresponds to one rotating disc. The second one, Σ, describes the intensity of the shear flow and directly defines the mean differential rotation. In our experiments $|\Delta| \leq |\Sigma|$, *i.e.,* we do not consider the case of co-rotating discs.

2.2. Induction measurements. An external magnetic field is applied and the induced field is measured inside the flow volume using a local Hall probe. Axial and transverse magnetic fields are generated using a set of induction coils located on either side of the cylindrical vessel – Fig. 1. This configuration is close, but not strictly equal to the Helmholtz geometry, so that the applied field is not completely uniform over the flow volume. Characterizing the inhomogeneity as the ratio of the magnetic field spatial variation (*rms* value) to the mean value, leads to values of about 18% for both axial or transverse applied fields. A toroidal field can also be applied. In this case, a strong DC current (of the order of 1000 A) is run from one flat end to the other in the flow vessel. The current is input by two pairs of copper electrodes located behind the driving discs, in the xOz plane – Fig. 1. If one assumes that the electrical current flowing along the axis has a uniform density in a cross-section, the applied azimuthal field increases linearly with the distance to the axis of the cylinder. A current of 1000 A generates an applied field of about 20 G at $r = R/2$, where most measurements are made. Note that with the currents of this order of magnitude one will not be able to neglect the field generated around the cables that connect the flow vessel to the DC power supply. In all experiments the applied field is less than 100 G, so that the interaction parameter, $N = \sigma B_0^2 L/\rho U = \sigma B_0^2 2R/\rho 2\pi R\Omega \sim 10^{-3}$, is quite small. We neglect the back-reaction of the magnetic field on the velocity field.

Magnetic measurements are performed inside the vessel using directional and temperature compensated Hall probes with a FW-Bell 9953 gaussmeter; the spatial resolution is 3 mm, with a frequency range from DC to 400 Hz. In order to study anisotropy effects, we have chosen to measure B at two different points in the median plane of the cylinder; the points are located at right angles, at a distance $r \approx R/2$ to the axis of the cylinder: point *1* is on the x-axis (at $\phi = \pi$), while point *2* is on the y-axis (at $\phi = \pi/2$). The signal from the Hall probe is registered for time intervals between 30 seconds and 2 minutes, using a National Instrument PXI-4472 digitizer at a rate of 1000 Hz and with a resolution of 23 bits. The mean magnetic field discussed in this article is computed as the time average over the entire time interval of the measurement. In the case of an axial applied field, we also measured the potentiel difference along the axis of the cylinder, using the same copper electrodes which input the DC current in the case of a toroidal applied field. The mean value only is recordered, using a Schlumberger 7061 micro-voltmeter.

3. Equations and induction mechanisms in von Kármán flows.

3.1. Induction equation. The evolution of the magnetic field in a flow of conducting fluid with a permittivity μ_0 and an electrical conductivity σ is governed by the induction equations

$$\partial_t \mathbf{B} = \nabla \times (\mathbf{v} \times \mathbf{B}) + \frac{1}{\mu_0 \sigma} \Delta \mathbf{B}, \qquad \nabla \cdot \mathbf{B} = 0 \ . \tag{1}$$

It states that the magnetic field dynamics results from the competitive action of induction and Joule diffusion ($\eta = 1/\sigma\mu_0$ is the magnetic diffusivity). The ratio of these two effects is measured by the integral magnetic Reynolds number Rm. In our case, Rm is moderate, typically less than 10, which is certainly below the threshold for dynamo action in this flow [18, 19]. The magnetic field equation must in principle be coupled with the fluid's dynamical equation which incorporates

the Lorentz force term. However, even in the presence of an applied field, the induced magnetic field remains small with an amplitude less than that of the applied field, so that the interaction parameter also remains small, less than 0.001, and the velocity field can be considered as fixed. The magnetic field in the flow is split into applied, external (earth field, cables, ...) and induced components: $\mathbf{B} = \mathbf{B}^{\mathrm{A}} + \mathbf{B}^{\mathrm{E}} + \mathbf{B}^{\mathrm{I}}$, and our aim is to describe $\mathbf{B}^{\mathrm{I}}$, when the applied field $\mathbf{B}^{\mathrm{A}}$ is axial, toroidal or transverse, for the von Kármán velocity fields $\mathbf{v}$ generated by the rotation of one or two discs. The magnetic field $\mathbf{B}^{\mathrm{E}}$ (between 0.5 and 1 G) is essentially smaller than the applied field $\mathbf{B}^{\mathrm{A}}$ (in the range 10 to 100 G) but as we shall show in section 5, it cannot always be neglected in the interpretation of the measurements.

Equation (1) must be supplemented with boundary conditions. In our case, the vessel containing the flow is made of stainless steel whose conductivity ($\sigma_{\mathrm{steel}} = 1.4 \cdot 10^6\,\Omega^{-1}\mathrm{m}^{-1}$) is three times smaller than that of Gallium; outside is air. The boundary condition is thus non-conducting at the flow wall. In this case, the boundary conditions for the magnetic field are that it should be continuous across the outer wall, where $\nabla \times \mathbf{B}$ has a zero normal component. In fact, the main condition is that of no outgoing current ($\mathbf{j} \cdot \mathbf{n} = 0$). We remark here that although the induction equation (1) is written for the magnetic field alone ($\mathbf{v}$ being given), the understanding of the full physical problem with real boundaries requires that one takes into account the complete set of equations. In particular, the electric potential Φ and the current $\mathbf{j}$, related through the Ohm's law $\mathbf{j} = \sigma(-\nabla\Phi + \mathbf{v} \times \mathbf{B})$ must be understood to interpret correctly the induction effects. This observation has lead to discovery of the 'BC-effect' described in section 6.

3.2. Induction mechanisms. We now discuss briefly how equation (1) can be used to predict and interpret the induction mechanisms in von Kármán flows.

In equation (1), the first r.h.s term represents the magnetic field produced by currents that are generated by the induction electromotive force (e.m.f.) $\mathcal{E} = \mathbf{v} \times \mathbf{B}$. Let us consider, for example, the induction due to differential rotation in the case of an axial applied field. This situation is that of counter-rotating discs and, as shown in Fig. 3*a*, the e.m.f's $\mathcal{E}$ induced near each disc are radial with opposite sign. The resulting currents take the shape of a solenoidal torus, Fig. 3*b*, so that the induced field is toroidal. This process is widely known as the ω-effect [1].

Another convenient way to understand the magnetic induction is to consider the deformation of magnetic field lines, initially imposed by the external field.

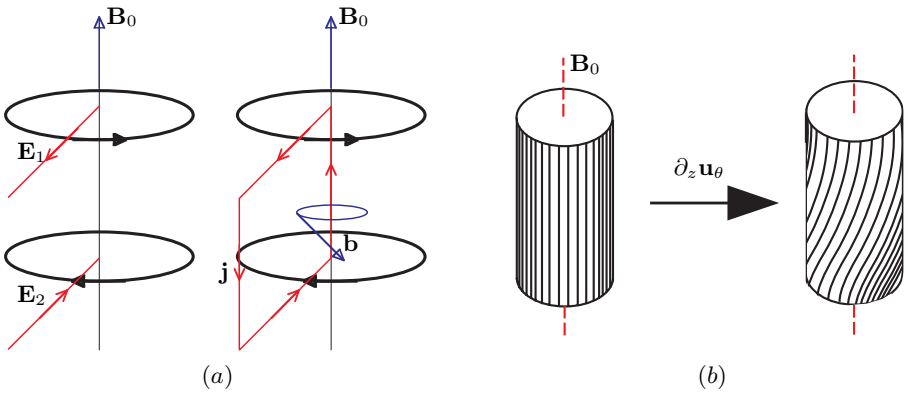

Fig. 3. Sketch of the omega effect produced by differential rotation, considered in (*a*) from the point of view of induction e.m.f. and induction currents, and in (*b*) from the point of view of magnetic field lines distorsion by velocity gradients.

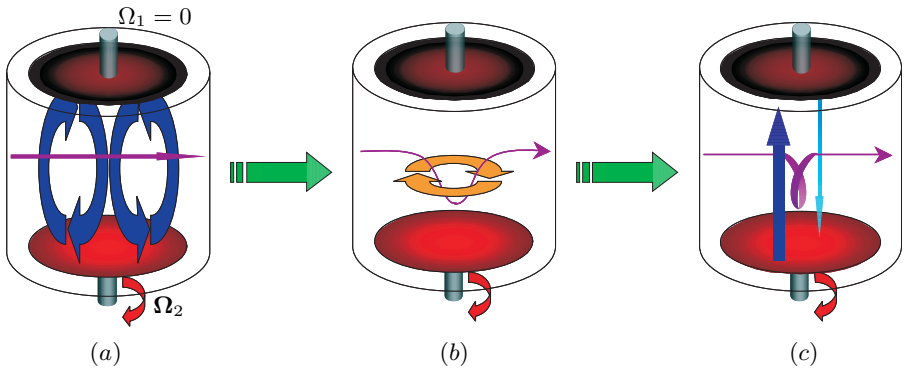

Fig. 4. Sketch of the 'alpha' or Parker effect produced by helical motion.

Indeed, as the fluid is incompressible, the induction term can be rewritten as $\nabla \times (\mathbf{v} \times \mathbf{B}) = -(\mathbf{v} \cdot \nabla)\mathbf{B} + (\mathbf{B} \cdot \nabla)\mathbf{v}$. The induction equation becomes

$$\partial_t \mathbf{B} + (\mathbf{v} \cdot \nabla)\mathbf{B} = (\mathbf{B} \cdot \nabla)\mathbf{v} + \eta \Delta \mathbf{B} \ , \tag{2}$$

which, save the diffusion term, has the form of the equation for a material fluid element. This analogy leads to the result that, in the limit of vanishing magnetic diffusivity, the magnetic lines are frozen in the fluid.

In equation (2) we note also that one easily recovers the two basic laws of induction used in classical electromagnetism of circuits: the $(\mathbf{v} \cdot \nabla)\mathbf{B}$ term represents the induction in a circuit with a fixed shape being moved in a inhomogeneous magnetic field, while the $(\mathbf{B} \cdot \nabla)\mathbf{v}$ term is the induction generated by changing the shape of a circuit immersed in a homogeneous magnetic field.

Turning to fluid motion, we note that the ω-effect discussed above corresponds to the twisting of axial magnetic field lines by the differential rotation of the flow – a $B_z \partial_z v_\phi$ term, see Fig. 3*b*. Another example is the well-known "stretch and twist" mechanism for a flow that is in strong helical motion. Consider in this case that a field is applied perpendicularly to the axis of the helical motion. The transverse gradients of the axial flow will 'stretch' the field lines along the axis of rotation, a "$(\mathbf{B} \cdot \nabla)\mathbf{v}$ " action – see Fig. 4*a*. This field loop, being inhomogeneous in the azimuthal direction, is then 'twisted' by the azimuthal flow, a "$(\mathbf{v} \cdot \nabla)\mathbf{B}$ " action – see Fig. 4*b*, *c*. The resulting induced magnetic field has an axial component. We call the Parker effect this two-step mechanism, converting a transverse magnetic field to axial, as it has been identified in Parker's original paper [16]. This effect will be discussed in section 6. The same mechanism is at the basis of the alpha effect that can develop in flows with scale separation [14].

We finally return to the fact that the experimental flow under consideration is strongly turbulent because of the very low value of the magnetic Prandtl number of Gallium: $\mathrm{Pm} = \nu/\eta = \mathrm{Rm}/\mathrm{Re}$, so Rm of order one are associated with Re exceeding 10^6. The total magnetic field should be written $\mathbf{B} = \mathbf{B}^{\mathrm{A}} + \mathbf{B}^{\mathrm{E}} + \mathbf{B}^{\mathrm{I}} + \mathbf{b}$, where the induced magnetic field is split into its mean ($\mathbf{B}^{\mathrm{I}}(\mathbf{r})$) and fluctuating ($\mathbf{b}(\mathbf{r}, t)$) components. If in the same manner the flow velocity field is split into its mean and fluctuating parts, $\mathbf{v}(\mathbf{r}, t) = \mathbf{U}(\mathbf{r}) + \mathbf{u}(\mathbf{r}, t)$, the induction equation governing the mean field,

$$\partial_t \mathbf{B}' = \nabla \times (\mathbf{U} \times \mathbf{B}') + \nabla \times \varepsilon + \eta \Delta \mathbf{B}' = 0, \qquad \mathbf{B}' = B^{\mathrm{A}} + \mathbf{B}^{\mathrm{E}} + \mathbf{B}^{\mathrm{I}}, \tag{3}$$

has an additional term, which comes from the effective electromotive force ε gen-

erated by the turbulent fluctuations

$$\varepsilon = \langle \mathbf{u} \times \mathbf{b} \rangle \ , \tag{4}$$

where the brackets denote a time-averaging. The contribution of such a term is essential in geometries, where scale separation is at work [14]. However, in von Kármán flows the scale separation is not clear and the question of the influence of turbulent velocity fluctuations regarding mean induction effects is open. Knowing the *rms* amplitude u of the velocity fluctuation, of the order of 35% of the mean U, one can estimate the relative importance of the local turbulent induction compared to the mean one as

$$\left[\frac{\mathbf{u} \times \mathbf{b}}{\mathbf{U} \times \mathbf{B}}\right] \sim \frac{u}{U}\frac{b}{B^{\mathrm{A}}} \sim \left(\frac{u}{U}\right)^2 \frac{\ell}{L}\,\mathrm{Rm} \ , \tag{5}$$

where ℓ is a scale characteristic of the turbulent fluctuations. For a turbulent decomposition of the kind discussed here, ℓ should be at least an order of magnitude smaller than L, so that one finds $\varepsilon < 10^{-2}\mathcal{E}$. We will discuss a possible contribution of the small scales as we analyze our measurements in the following sections.

3.3. Symmetry arguments. The von Kármán geometry has many symmetries and it proves to be worthwhile to take some of them into account when analyzing induction measurements. Let us note $\mathbf{B}\{P, \Omega_1, \Omega_2, \mathbf{B}_0\}$ as the magnetic field induced at point P when motor *1* rotates at an angular velocity Ω_1, motor *2* rotates at an angular velocity Ω_2 and an external field $\mathbf{B}_0$ is applied. If a transformation $\mathcal{T}$ is applied to the setup (reflexion, rotation or else), the induced field and the flow parameters are related by

$$\mathcal{T}(\mathbf{B}\{P, \Omega_1, \Omega_2, \mathbf{B}_0\}) = \mathbf{B}\{\mathcal{T}(P, \Omega_1, \Omega_2, \mathbf{B}_0)\}. \tag{6}$$

We give below three examples of general results that can be drawn using this relationship. These examples will help us to analyze some properties of the measured induced field.

As a first example, let us consider the case when the flow is generated by the counter-rotation at equal speeds, a transverse field is applied along the x-axis and the induced field is measured in the mid-plane on the x-axis (point *1*). In this case, we show that two components of the induced field are necessarily null. Indeed, let $\mathcal{T}$ be a rotation of angle π around the x-axis and P a measurement point on that axis. Under this transformation, one has

$$\mathcal{T}(B_x) = B_x, \ \ \mathcal{T}(B_y) = -B_y, \ \ \mathcal{T}(B_z) = -B_z \ , \tag{7}$$

for the induced field, while the flow parameters are changed into

$$\mathcal{T}(P, \Omega_1, \Omega_2, \mathbf{B}_0) = (P, \Omega_2, \Omega_1, \mathbf{B}_0) \ . \tag{8}$$

As a result, $-B_y\{P, \Omega_1, \Omega_2, \mathbf{B}_0\} = B_y\{P, \Omega_2, \Omega_1, \mathbf{B}_0\}$, so that $B_y = 0$ at point $P \in Ox$ when $\Omega_1 = \Omega_2$, and $B_z = 0$ in the same manner.

Now let us consider the case of a transverse field still applied along the x-axis, with the measurement made at a point P located on the y-axis (point *2*). We show that the induced component of the magnetic field in the axial direction must be even when the rotation speeds of disc *1* and disc *2* are interchanged. To wit, we use $\mathcal{T}$ as a rotation of angle π around the y-axis. In this case

$$\mathcal{T}(B_z) = -B_z \quad \text{and} \quad \mathcal{T}(P, \Omega_1, \Omega_2, \mathbf{B}_0) = (P, \Omega_2, \Omega_1, -\mathbf{B}_0) \ . \tag{9}$$

Using the fact that the induction equation is linear in the applied magnetic field, one finds

$$B_z\{P,\Omega_1,\Omega_2,\mathbf{B}_0\} = B_z\{P,\Omega_2,\Omega_1,\mathbf{B}_0\}, \qquad P \in Oy\ . \tag{10}$$

Finally, for the same applied field, we consider the induction at a point P located in the median xOy plane. We show that the induced field must be odd under the reversal of discs rotation, if point P is located on the Oy-axis. Indeed, let transformation $\mathcal{T}$ be a reflexion with respect to the xOy plane. Remembering that the magnetic field is a pseudo-vector and that under the transformation $\mathcal{T}$ the coordinate system is reversed, one finds:

$$\mathcal{T}(B_z) = B_z \quad \text{and} \quad \mathcal{T}(P,\Omega_1,\Omega_2,\mathbf{B}_0) = (P,-\Omega_2,-\Omega_1,-\mathbf{B}_0)\ . \tag{11}$$

Using again the linearity of the induction equation, one gets

$$B_z\{P,\Omega_1,\Omega_2,\mathbf{B}_0)\} = -B_z\{P,-\Omega_2,-\Omega_1,\mathbf{B}_0\}, \qquad P \in xOy\ , \tag{12}$$

which together with relationship (10) shows that the axial component of the induced magnetic field transforms as

$$B_z\{P,\Omega_2,\Omega_1,\mathbf{B}_0\} = -B_z\{P,-\Omega_2,-\Omega_1,\mathbf{B}_0\}, \qquad P \in Oy\ . \tag{13}$$

Our measurements are in agreement with these very general symmetry considerations which do not depend upon a particular 'induction mechanism'.

4. Poloidal (axial) field. We consider here the magnetic response of the flow to an external field applied parallel to the axis of rotation of the driving discs. The external poloidal field is induced by two coils located at each end of the flow cylinder (see Fig. 1) so that $\mathbf{B}^{\mathrm{A}} = (0,0,B_0^{\mathrm{A}})$ with B_0^{A}=24 G.

4.1. Azimuthal induction. We first study the azimuthal component of the induced field, which is mainly produced by differential rotation; indeed the azimuthal projection of the induction equation (2) yields to leading order and assuming stationarity

$$\eta(\Delta B^{\mathrm{I}})_\phi \approx B_0^{\mathrm{A}}\partial_z v_\phi\ . \tag{14}$$

We show in Fig. 5*a* the induced toroidal field measured at point *2* for counter-rotating discs. The behaviour is similar at point *1*, as expected from the axisymmetry of the experiment. From Eq. (14) one expects that the induced field scales linearly with the velocity gradient and thus with Ω, as indeed observed. For $\Omega = 24$ Hz, the amplitude of induced azimuthal magnetic field reaches about 30% of the applied axial field. The ratio of the magnitude of the induced field to the applied one actually defines a local measurement of an intrinsic magnetic Reynolds number $\mathrm{Rm}^{\mathrm{i}} = B_\phi^{\mathrm{I}}/B^{\mathrm{A}}$; in this case $\mathrm{Rm}^{\mathrm{i}} \sim 0.3$ is in agreement with previous observations [12]. Fig. 5*b* shows the induced azimuthal field, when the rotation rate difference $\Delta = \Omega_2 - \Omega_1$ is varied, with the sum $\Omega_1 + \Omega_2$ kept constant at 24 Hz. One observes that the induction effect rapidly decreases when $|\Delta|$ increases. This effect is subtle; the induced azimuthal magnetic field is concentrated in the shear layer, where the differential rotation is localized. Although the axial extension of this layer is about half of the distance between the discs, its position is quite unstable under small deviations of Δ from zero [20]. As a result, the measured induced field decreases sharply when the discs are no longer rotating at equal speeds. The generation of the toroidal magnetic field corresponds to the production of an electrical current along the cylinder's z-axis which closes up through the cylinders walls and boundary layers. Thus, a difference of potential should arise

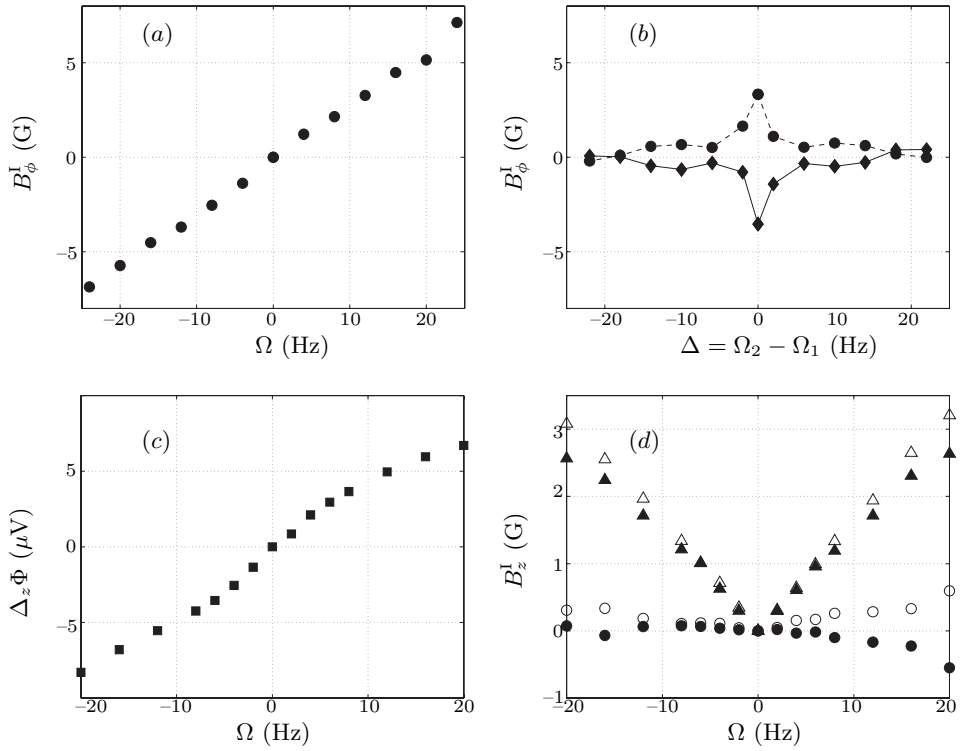

Fig. 5. Induction measurement for an axial applied field: (*a*) azimuthal component of $B^{\rm I}$ for counter-rotating discs with equal rotation rates Ω, (*b*) azimuthal component of $B^{\rm I}$ for counter-rotating discs as a function of rotation rates difference Δ, for $\Sigma = 12$ Hz (dashed line) and $\Sigma = -12$ Hz (solid line), (*c*) axial potential difference, (*d*) axial component of $B^{\rm I}$ for counter-rotating discs with equal rotation rates Ω, measured at points *1* (filled symbols) and *2* (open symbols) and at two distances from the axis: 3 cm (triangles), 7 cm (circles).

between the flat ends of the cylinder and could form an integral characteristic of the toroidal field generation. The total potential difference across the cylinder, measured for the applied axial magnetic field $B_0 = 24\,\mathrm{G}$ as a function of Ω is shown in Fig. 5*c*. Two remarks can be made. First, the dependence $\Delta\Phi(\Omega)$ is not as linear as the curve for $B_\phi(\Omega)$ in Fig. 5*a*. This can be explained by the integral character of potential measurements which is affected by the general expulsion of the applied field from the flow core, as Ω increases. Secondly, the measured value of the potential difference for given Ω can be compared to an estimation using simple electrodynamic considerations. The induced current can be estimated from the value of the measured induced field at $\Omega = 10$ Hz, using the Ampère's law. The potentiel difference is then estimated, assuming that this current flows through the electrical resistance of the fluid inside the vessel. This yields $\Delta\Phi \simeq 500$ μV. The measured value for $\Omega = 10$ Hz is 90 μV. This lower value could be explained by the fact that the region where the toroidal field is induced, is essentially smaller than the distance between the electrodes (the shear layer thickness is roughly one third of the distance between the electrodes).

4.2. Axial induction. Another interesting feature in this configuration is the axial induction due to the axial stretching near the stagnation point, separating the poloidal vortices produced by the counter-rotating discs, as shown in Fig. 2*b*. The corresponding source term in the induction equation (2) is $B^{\rm A}\partial_z v_z$. Fig. 5*d* shows the axial induced field as a function of Ω, respectively measured on the x-

axis (at $\phi = \pi$, filled symbols), and on the y-axis (at $\phi = \pi/2$, open symbols). This effect has a linear contribution which dominates at low Rm. In addition, since it is created by the axial flow, it does not depend on the direction of rotation of the disc, as observed in Fig. 5*d*. It is also concentrated in the neighbourhood of the stagnation point and thus strongly depends on the distance of the measurement point to the axis of the flow. To wit, two different radial locations of the probe have been studied: 3 cm from the axis (triangles) and 7 cm from the axis (circles). One can see that the axial induction near the axis is strong and independent of ϕ and that it is much smaller when measured far from the axis. In this last case, the effect is very sensitive to the precise location of the probe, whose depth is set with a 5 mm precision (it may explain the difference between measurements made at different angles ϕ (circles in Fig. 5*d*)).

5. Toroidal field In this section we study the transformation of an externally applied toroidal magnetic field generated by a strong axial electrical current through the fluid. Note that the toroidal field generated in this manner is uniform along the axis of the cylinder. It is somewhat different from the azimuthal field induced by differential rotation which is localized in the shear layer, as described in previous section.

Fig. 6 *a*,*b*,*c* show the axial induced field at point *1*, respectively, for disc *1* rotating, counter-rotation and disc *2* rotating. Fig. 6 *d*,*e*,*f* show corresponding measurements at point *2*. The value of the toroidal magnetic field induced by the axial current $I_0 = 1000$ A at the points where the probe is located is $B_\phi^{\rm A} = 20$ G. The external magnetic field was $\mathbf{B}^E \approx (-0.1, 0.5, 0.6)$ G (in cylindrical coordinates (B_r, B_ϕ, B_z)) at point *1* and $\mathbf{B}^{\rm E} \approx (0.5, 0.1, 0.6)$ G at point *2* ($B^{\rm E}$ comes from the earth magnetic field and the magnetic field of the cables connectig the flat ends of the vessel to the DC power supply). Comparison of upper (point *1*) and lower (point *2*) rows in Fig. 6 clearly shows that the induced field behaviour strongly depends on the location of the measurement point. Moreover, the curves display

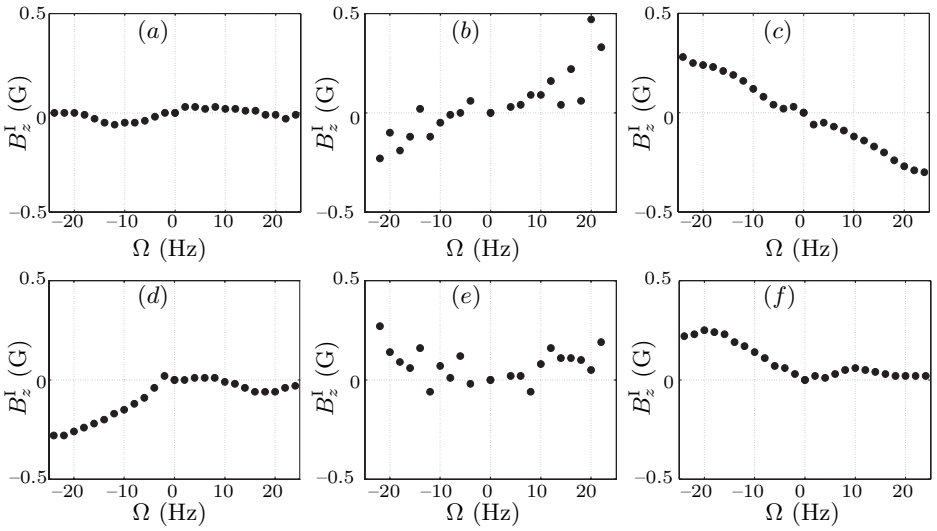

Fig. 6. Induced axial magnetic field when a 1000 A axial current passes axially through the vessel. Measurements are made at point *1* (upper row) and point *2* (lower row) for the flow driven by the rotation of disc *1* alone (left panels), disc *2* alone (right panels), or both counter-rotating discs (center).

the absence of similarity when some evident symmetries could be expected: the induced field at point *1* with disc *1* rotating disappears when disc *2* is rotated, (Fig. 6 *a*,*c*), and at point *2* the induced field shows no symmetry with respect to the direction of rotation of the discs (Fig. 6 *d*,*f*).

In order to analyze these observations, we return to the induction equation. Taking into account the axisymmetry of the mean flow (all ϕ derivatives vanish), the axial projection of equation (1) yields in the stationary case and for the mean fields

$$\eta(\Delta B)_z = r^{-1}\partial_r \left(r \left(B_z v_r - B_r v_z\right)\right). \tag{15}$$

If the applied field is purely toroidal (neglecting B^{E}), it can be seen in equation (15) that it cannot contribute to the induced axial field, unless it also induces a radial field. The radial projection of equation (1) for the mean fields yields

$$\eta(\Delta B)_r = \partial_z \left(B_r v_z - B_z v_r\right) \ . \tag{16}$$

It can be shown [1] that the coupled set of equations (15) and (16) leads to $B_r = B_z = 0$. No poloidal field can be sustained from a mean toroidal field. Note that this result is no more than an expression, in our specific case, of a more general result stating that no axisymmetric magnetic field can be generated by an axisymmetric velocity field (Cowling's theorem).

Therefore, in the case of a completely toroidal applied field, only the turbulent term $\nabla \times \langle \mathbf{u} \times \mathbf{b} \rangle$, which was neglected in equations (15) and (16) could contribute to the induced poloidal field. This term is mainly related to the small scale helicity of the flow. We make an asumption that this small scale helicity has the same symmetry properties as the large scale helicity of the flow. The helicity created by one disc or the other is of the same sign: the transformation disc *1* $\rightarrow$ disc *2* changes the sign of the centrifugal pumping and the sign of the azimuthal flow at the same time. Therefore, this helicity also exists, even with a stronger contribution, when the discs are counter-rotating. From these features we can derive the expected symmetries of the turbulent term. It is odd in $\Omega \rightarrow -\Omega$ and even with respect to a change of disc: the sign of induced B_z^{I} should depend on the sign of Ω only. Furthermore, $B_z^{\mathrm{I}}(\Omega)$ dependence should be similar for one and two rotating discs and the magnitude of this term should be the same at measuring points *1* and *2* as small scale turbulence is supposed to be homogeneous. No trace of a contribution with these properties is visible in our data: at point *2* $B_z^{\mathrm{I}}(\Omega)$ changes the sign with disc exchange in one-disc data (Fig. 6 *d*,*f*) and is absent in two-disc data (Fig. 6*e*). At point *1* (Fig. 6 *a*,*b*,*c*), the behavior is again different but does not either correspond to the expected symmetries. We must, therefore, conclude that no evidence is found in our experimental data of a contribution of turbulent fluctuations in the conversion from a toroidal field into a poloidal field. The induced axial field that is seen on the data has to originate from the external field B^{E} that has been neglected until now. This field is mainly transverse (orthogonal to the axis of the cylinder) but is probably far from homogeneous in the axial direction. The interpretation of Fig. 6 based on mechanisms in which the induced field is generated from B^{E} is thus not easy. In the next section we study in detail the response of the flow to an applied magnetic field whose orientation is perpendicular to the axis of rotation. At the end of this section, we will come back to some features of the data in Fig. 6.

6. Transverse field. Now, we apply a field B_x^{A} =43 G, perpendicular to the axis of rotation, in order to investigate the flow response when the axisymmetry is broken. Such a field is generated by two induction coils set on each side of

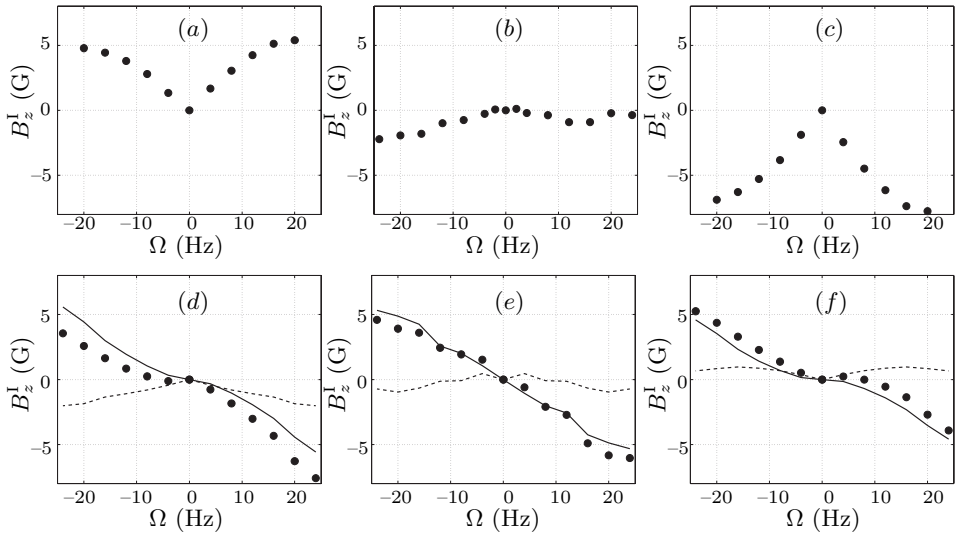

Fig. 7. Induced axial magnetic field for a transverse applied field along the x-axis. Measurements are made at point *1* (upper row) and point *2* (lower row), for the flow induced by the rotation of disc *1* alone (left panels), disc *2* alone (right panels), or both counter-rotating discs (center). In the lower row (point *2*), the measurements are split into their odd (solid line) and even parts (dashed line).

the flow vessel aligned with the x-axis, Fig. 1. This is an interesting case to be studied because numerical simulation of the kinematic dynamo problem in this geometry has shown that the magnetic field induced by dynamo action has a strong component in this transverse direction [10]. Although the dynamo cycle in this geometry is not known, it must involve the generation of an axial field component from a transverse applied field.

Fig. 7 *a*,*b*,*c* show the axial induced field at point *1*, respectively, for disc *1* rotating, counter-rotation and disc *2* rotating. Fig. 7 *d*,*e*,*f* show corresponding measurements at point *2*. One can first notice that the behaviour is clearly different at the two measurement points. This is to be expected since the applied transverse field breaks the axisymmetry of the experiment. For measurements with only one disc rotating, the axial induced field at point *1* is linear in Ω and even with respect to a reversal of the direction of rotation of the disc; it is odd with respect to disc exchange (disc *2* rotates instead of disc *1*). On the other hand, at point *2* it is non-linear in Ω and odd with respect to a reversal of the direction of rotation of the disc, while it is even with respect to disc exchange. In the case of counter-rotating discs, the behaviour is again different. Some of these properties are direct consequences of the symmetry arguments given in section 3.3, independent of the induction mechanisms.

6.1. Linear bulk effects. In order to analyze our experimental results, let us consider the axial projection of the induction equation (2)

$$\partial_t B_z = (\mathbf{v}\cdot\nabla)B_z + (\mathbf{B}\cdot\nabla)v_z + \eta\Delta B_z \tag{17}$$

The applied field B^{A} has no axial component, so all source terms, involving B_z, will not contribute to induce the field to lowest order. Thus, only two terms remain in the source terms of equation (17). Using a cylindrical decomposition of $(\mathbf{B}\cdot\nabla)v_z$, these two terms can be written: $B_\phi\partial_\phi v_z$ and $B_r\partial_r v_z$. The first one vanishes because of the flow axisymmetry. In the second one, the tranverse applied field

(aligned with the x-direction) acts through its radial component $B_r^{\rm A} = B_0 \cos\phi$. The cosine factor generates the difference between the measurements at points *1* and *2*.

At point *1* ($\phi = \pi$, cf. Fig. 1), an induced field is expected from the $B_r \partial_r v_z$ source term. In the case of one rotating disc, it is linear with Ω because it is proportional to the velocity gradient and it is even with respect to reversal of the rotation rate because it is related to the axial flow, which does not depend on the sign of Ω. For both figures 7*a* and *c* and for each direction of rotation, the slope $\left|\partial B_z^{\rm I}/\partial\Omega\right|$, measured in the interval [−10 Hz, 10 Hz], has the same value (0.38 G/Hz) within 3%. For larger values of Ω, a saturation effect is observed. It can be explained by the expulsion of the applied transverse field by the toroidal velocity [13]. In addition, the induced field should be odd with respect to a change of disc (reversal of the pumping flow), which is the case in the experimental data.

Turning to the counter-rotating discs case, the first symmetry argument presented in section 3.3 states that no axial induced field should be measured. This is indeed what is shown in Fig. 7*b*, within experimental errors. It can also be explained by regarding the counter-rotation flow as a sum of two cells, each one equivalent to a one-disc flow field. As the induced field in the one-disc case is odd with respect to disc exchange, the contribution of each half of the flow have opposite sign and cancel in the median plane where the probe is located. Actually, the null mean value of the axially induced field is a result of time averaging. To wit, we show in Fig. 8*a* the time signal $B_z(t)$ for Ω = 12 Hz (corresponding to one point of Fig. 7*b*). One obtains a time averaged value close to zero, when the measurement is averaged over a long enough time interval, as described in section 2. On shorter time scales (of few seconds), the average is not zero anymore, corresponding probably to a non-stationary symmetry-breaking of the flow, as the shear layer located on average on the mid-plane oscillates irregularly about the mid-plane. This behaviour of the shear layer has been observed in a water prototype of this experiment [20]. As mentioned in section 4.1, if one disc rotates a little faster than the other, the shear layer moves away from the mid-plane. Therefore, it is interesting to compare Fig. 8a with the time signal of the induced axial field in the case, where $\Delta = \Omega_2 - \Omega_1 \neq 0$. In Fig. 8*b*, the upper curve corresponds to the case with Ω_1=13 Hz and Ω_2=11 Hz, and the lower one corresponds to the opposite case, Ω_1=11 Hz and Ω_2=13 Hz. One observes a non zero induced field, due to the displacement of the shear layer, thus breaking the symmetry of the flow. Therefore, symmetry arguments no longer apply and the induced field from

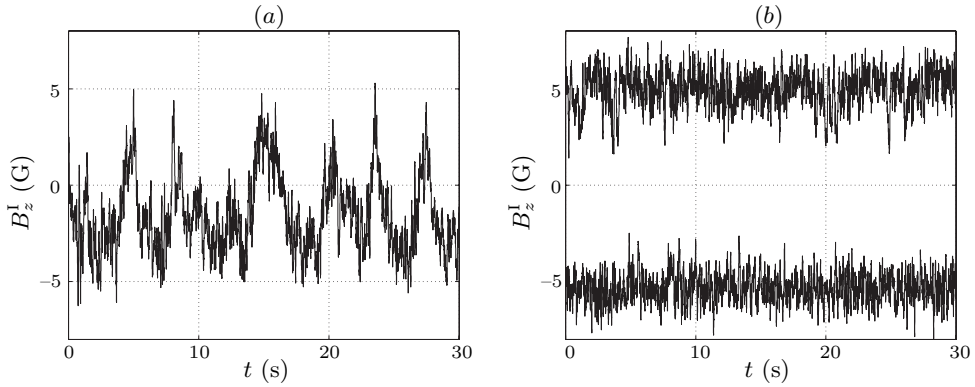

Fig. 8. Time variation of the induced axial magnetic field for a transverse applied field along the x-axis; measurement at point *1*, for Σ = 24 Hz. In (a) the discs rotate at equal speeds ($\Delta = 0$); in (b) they are counter-rotating at slightly different speeds ($\Delta = \pm 2$ Hz).

Table 1. Source terms for a radial induced field at point *2* when a transverse field is applied along the x-axis.

$v_\phi \partial_\phi B_r^{\rm A}$	yes	$\partial_\phi B_r^{\rm A} = B_0 \sin\phi$ maximum at point *2*
$v_r \partial_r B_r^{\rm A}$	no	$B_r^{\rm A}$ does not depend on r
$v_z \partial_z B_r^{\rm A}$	no	$B_r^{\rm A}$ does not depend on z
$B_\phi^{\rm A} \partial_\phi v_r$	no	axisymmetry of the flow
$B_r^{\rm A} \partial_r v_r$	no	$B_r^{\rm A}$ vanishes at point *2*
$B_z^{\rm A} \partial_z v_r$	no	$B_z^{\rm A} = 0$

the dominant half of the cylinder can be measured in the mid-plane. By comparing Fig. 8*a* and *b*, one can observe that in the case of counter-rotation, the non stationnary induced field reaches values close to the mean value measured with $|\Delta| = 2$ Hz. Thus, the amplitude of the oscillation of the shear layer at $\Delta = 0$ is of the same order of magnitude as the displacement of this layer obtained with $|\Delta| = 2$ Hz.

6.2. Non-linear bulk effect. At point *2*, with the radial component of $\mathbf{B}^{\rm A}$ being zero ($\phi = \pi/2$), no linear contribution is expected. But if there is some induced radial field in a first step, one can expect an induced axial field from the source term $B_r^{\rm I} \partial_r v_z$. The analysis of the possible source terms for an induced radial field is presented in Table 1 for each term we indicate, if it can contribute and why. Thus, the only contributing term for the induced axial field at point *2* is of type $B_r^{\rm I} \partial_r v_z \simeq v_\phi B_0 \sin\phi \; \partial_r v_z$. This term, involving at the same time the toroidal velocity and the axial pumping, acting on an initial transverse field, is the Parker effect described in section 3.

In the case of one rotating disc, this effect has been observed in another experiment of the same type using liquid sodium [17] at a higher magnetic Reynolds number (Rm up to 25). It is also clearly visible in Fig. 7*d*,*f*. It has the same symmetries as the helicity of the flow: odd with Ω and even with respect to disc exchange. Indeed, the third symmetry argument mentioned in section 3.3 (equation (13)) shows that at this point only odd contribution with Ω can exist. As a result, the effect is identified more clearly when the measurements are split into even and odd parts ($f_{\rm even}(\Omega) = (f(\Omega) + f(-\Omega))/2$, dashed lines in Fig. 7*d*,*e*,*f* and $f_{\rm odd}(\Omega) = (f(\Omega) - f(-\Omega))/2$, solid lines). We can then observe that the induction curves in the case of one rotating disc (Fig. 7*d*,*f*) consist of a dominant odd part,

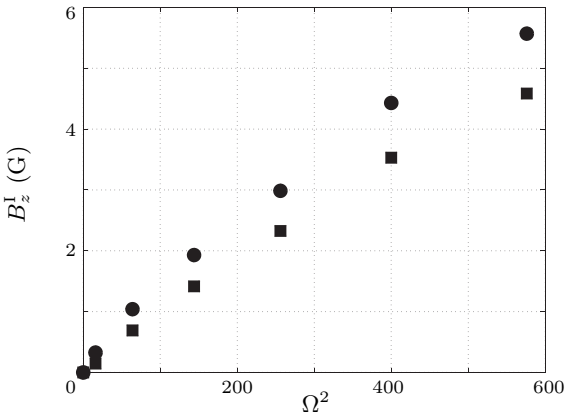

Fig. 9. Parker-induced axial field (odd component of $B_z^{\rm I}$) for an applied transverse field $B_x^{\rm A}$, plotted versus the square of disc rotation rate; (squares): only disc *1* rotates (circles): only disc *2* rotates.

even with respect to disc exchange, as expected (and in agreement with the symmetry property shown in equation (10)), and of a minor even part, behaving as at point *1*. This contribution is due to the fact that in these particular measurements and for technical reasons the real location of the probe at point *2* is not exactly at $\phi = \pi/2$ (there is a shift by 19°), therefore, a small contribution of the linear induced field remains.

The main characteristic of the odd part is that, being the result of a two-steps induction process, it should vary quadratically with the rotation rate of the discs. This is illustrated in Fig. 9, where the odd contribution is plotted versus Ω^2. When Rm increases, a saturation effect can be seen, corresponding to the expulsion of the applied field by the toroidal vortex, as was the case for the linear effect observed at point *1*. This saturation has also been observed in various experiments, where the alpha/Parker mechanism is involved [3, 17].

6.3. Linear boundary condition effect. When the flow is driven by the counter-rotation of two discs, one expects a Parker effect generated by the swirling motion on either side of the median plane. Since the magnetic diffusive length is large, the effect should thus be measurable in the median plane – the effects add up since the helicity has the same sign in each swirling shell. However, it can be seen in Fig. 7*e* that the odd part of the induced field in the case of counter-rotation is linear with Ω, and not quadratic as in the Parker effect. In this case, the induced axial field is produced *via* another mechanism, associated with the discontinuity of

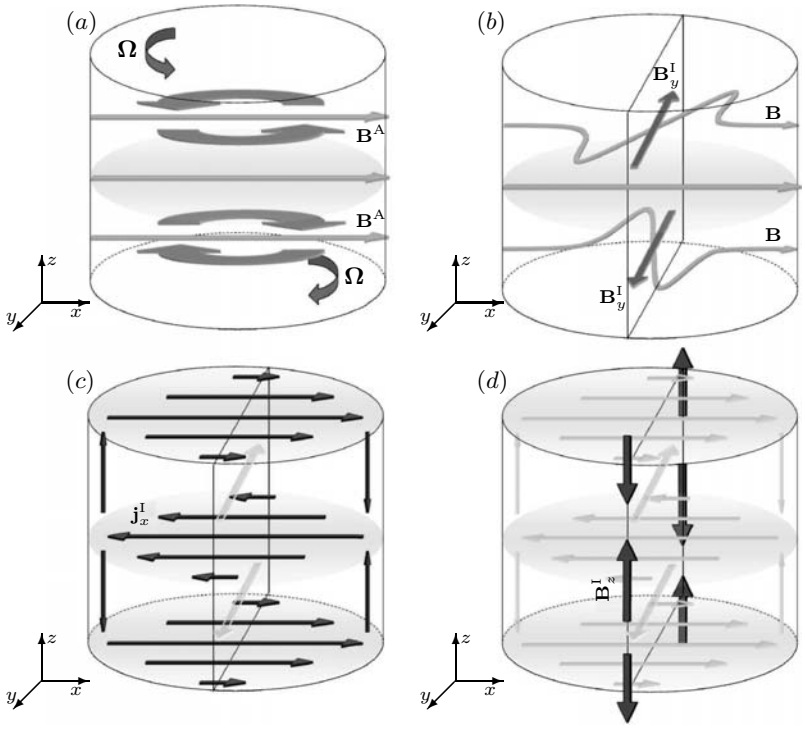

Fig. 10. Sketch of the BC-effect for a transverse applied field $\mathbf{B}^{\mathrm{A}}$ along the x-axis; (a) initial field and discs rotations; (b) radial differential rotation creates a perpendicular induced component $\mathbf{B}^{\mathrm{I}}_y$; (c) induced current sheets $\mathbf{j}^{\mathrm{I}}_x$ responsible for the generation of $\mathbf{B}^{\mathrm{I}}_y$; ($d$) axial field $\mathbf{B}^{\mathrm{I}}_z$ generated at the wall $y = \pm R$, due to the discontinuity in electrical conductivity.

the electrical conductivity at the flow vessel, in a manner similar to the situation reported in [21]. In the following, we describe it in detail for our genometry.

The process is sketched in Fig. 10. It is best explained when looking at the currents, resulting from the magnetic induction in the bulk. On either sides of the mid-plane an induced radial field is generated from the transverse applied field, of the form $v_\phi \partial_\phi B_r^{\mathrm{A}} = v_\phi B_0 \sin\phi$ (see Table 1 and Fig. 10*a*). Because of the sine factor, this field is mainly presented on the y-axis, parallel to it. The orientation of this induced field is reversed in each side of the median plane because of the v_ϕ factor (see B_y^{I} in Fig. 10*b*). A sheet of the induced electric current in the mid-plane is associated with this field, parallel to the x-axis (see j_x^{I} in Fig. 10*c*). Now, the insulating boundary conditions at point *2* generate a discontinuity of the tangential current, so that an axial field must be created in the vicinity of this point (B_z^{I} in Fig. 10*d*). It corresponds to the measured axial field in Fig. 7*e*. As it is related to the current, which increases linearly with Ω, it should also be of a first order effect, linear in Ω. This effect is absent at point *1*, where the electric current is normal to the boundary.

The sketch in Fig. 10*d* illustrates how the induced axial field varies with the z-coordinate. This field has one direction in the central part of the cylinder and the opposite one near each flat-end. This is due to the fact that the electrical current sheet, present in the mid-plane, loops back at each end of the cylinder, creating in these regions a sheet of the current of opposite sign. To wit, we have measured B_z^{I} versus z, just outside the vessel at a series of points ($x = 0$, $y = R + 2$ cm, $0 \leq z \leq 16$ cm, again in the case of two counter-rotating discs at equal speeds. The result is shown in Fig. 11: B_z^{I} indeed changes the sign at $z \sim 10$ cm, to reach clear negative values for $z \simeq 15$ cm.

As a final comment to the measurements made in the presence of an external transverse field, we note that we have been able to explain all the characteristics in Fig. 7 using only the induction generated by the mean flow. If turbulent fluctuations actually give a contribution to the mean induction, we have not found a clear evidence for it, either while analyzing the values of the induced magnetic field or its symmetry properties. At point *1*, the observed symmetries of the induced field do not correspond to the symmetries expected for the turbulent contribution. At point *2*, the symmetries correspond, but all features can be explained without having to invoke a turbulent source term.

6.4. A further comment on section 5. Resting upon the understanding developed in this section, we can return to the measurements reported in section 5. We concluded there that the observed induced field was due to the external field

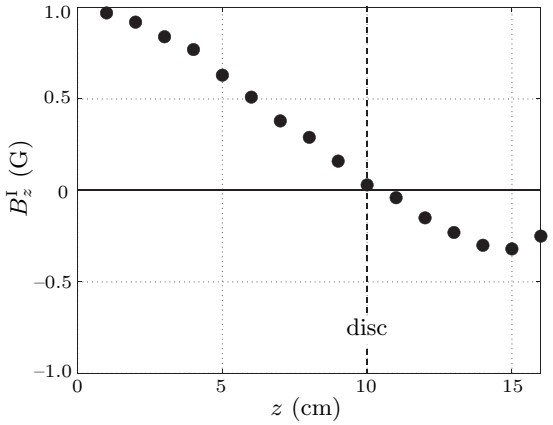

Fig. 11. Transverse applied field B_x^{A} for counter-rotating discs at $\Omega = 12$ Hz. The axial component of the induced field is measured outside the vessel, from the mid-plane to one end of the vessel, ($x = 0, y = R + 2$ cm, $0 \leq z \leq 16$ cm).

B^{E}. This field, though probably not homogeneous along the z-axis, is observed to be mainly parallel to the y-axis, at least in the mid-plane. Therefore, one would expect for the induced field a behaviour similar to what was observed in the case of a transverse applied field, except that points 1 and 2 should be exchanged. For counter-rotating discs, one indeed observes a linear induction effect at point *1* (Fig. 6*b*) and almost no effect at point *2* (Fig. 6*e*). The behaviour is more difficult to explain for the cases with a single rotating disc, even under the hypothesis of a transverse field B^{E}. It may be due to the fact that this field is not homogeneous along the z-axis.

7. Concluding remarks. We have observed that in the presence of an externally applied field the magnetic field induced in the flow has bulk contributions as well as boundary contributions. Although the production of the induced field is localized in regions where the velocity gradients or conductivity gradients are essentially large, their influence is felt over the entire flow volume because of the large magnetic diffusion length.

Induction, bulk effects. We have described the omega (linear) and Parker (quadratic) effects in swirling flows of liquid Gallium at moderate magnetic Reynolds numbers ($\mathrm{Rm} < 10$). These bulk effects dominate in different parts of the flows, showing that the induction is localized within the limits of a large diffusion scale unavoidable in liquid metals. Recent measurements in liquid Sodium in flows with the same geometry [17] show that these two effects can cooperate. It opens up the possibility of an $\alpha\omega$ dynamo cycle in the von Kármán flow generated by the counter-rotation of the discs. This cycle is in agreements with the kinematic dynamo simulations of Marié *et al.* [10], where the dynamo field is transverse. We have observed that the poloidal to toroidal conversion is very efficient, but found no evidence of a symmetric conversion of a toroidal field into a poloidal one. Although this is expected from the laminar mean flow, a contribution from turbulent fluctiations could not be *a priori* ruled out. In fact, a contribution from turbulence could have been expected because the small scale helicity is related to the large scale one [22, 23]. This has prompted us to look for induction characteristics with the symmetry of the turbulent source term. Our finding is that at the Rm and Re studied clear effects of turbulence are not observed.

Induction, boundary condition effect. We emphasize that the boundary conditions are important in real experimental flows. The 'new' BC-effect described in this paper stems from the discontinuity of the electric conductivity. In the case of the von Kármán flow, it is important to note that the magnetic field it generates has the same symmetries as the one produced *via* the non-linear Parker effect. This effect also appears as soon as the conductivity at the flow wall is not strictly equal to that of the fluid. Bulk effects are thus enhanced if the moving fluid is surrounded with a layer of fluid at rest, as in the Riga and Karlsruhe experiments. Finally we note that this 'new' boundary effect can be derived directly from the induction equation if one takes into account electric conductivity inhomogeneities from the start. In such a case, the induction equation reads

$$\partial_t \mathbf{B} = \nabla \times (\mathbf{v} \times \mathbf{B}) + \frac{1}{\mu_0 \sigma} \Delta \mathbf{B} + \frac{1}{\mu_0 \sigma} \nabla \ln \sigma \times (\nabla \times \mathbf{B}) \ , \tag{18}$$

the boundary condition being now that of vanishing magnetic field at infinity. The existence of a gradient of the electric conductivity may play an essential role in dynamo mechanism, either in natural situations or laboratory experiments. In the laboratory, conductivity gradients within the flow are very hard to establish, but they are plausible in natural dynamos, where the temperature of

the medium has huge variations. For example, in a spherical geometry with a radial gradient of conductivity, the 'BC-effect' can amplify a poloidal induced field. This could help the toroidal-poloidal conversion in natural dynamos, where the alpha-effect alone might not be sufficient.

Acknowledgments. We thank ISTC for support under project #2021. P.F. and S.K. thank the Laboratoire de Physique at ENS-Lyon for their hospitality. M.B., R.V., P.O. and J.-F.P. acknowledge many fruitful discussions with all the members of the VKS collaboration: A. Chiffaudel, F. Daviaud, S. Fauve, L. Marié, F. Pétrélis, and F. Ravelet.

REFERENCES

[1] H.K. Moffatt. *Magnetic Field Generation in Electrically Conducting Fluids* (Cambridge University Press, Cambridge, 1978).

[2] A. Gailitis, et al. Detection of a flow induced magnetic field eigenmode in the Riga dynamo facility. *Phys. Rev. Lett.*, vol. 84 (2000), pp. 4365–4368.

[3] R. Stieglitz, U. Müller. Experimental demonstration of a homogeneous two-scale dynamo. *Phys. Fluids*, vol. 13 (2001), no. 3, pp. 561–564.

[4] Y. Zeldovich, A. Ruzmaikin, D. Sokoloff. *Magnetic Fields in Astrophysics* (Gordon and Breach, N.Y., 1983).

[5] G.O. Roberts. Dynamo action of fluid motions with two dimensional periodicity. *Phil. Trans. Roy. Soc. London A.*, vol. 266, (1970), p. 535.

[6] R. Stieglitz, U. Müller. Experimental demonstration of a homogeneous two-scale dynamo. *Magnetohydodynamics*, vol. 38 (2002), no. 1-2, pp. 27–33.
A. Tilgner, F.H. Busse. Simulation of the bifurcation diagram of the Karlsruhe dynamo. *Magnetohydodynamics*, vol. 38 (2002), no. 1-2, pp. 35–40.
K.-H. Rädler, M. Rheinhardt, E. Apstein, H. Fuchs. On the mean–field theory of the Karlsruhe dynamo experiment *Magnetohydodynamics*, vol. 38 (2002), no. 1-2, pp. 41–94.
F. Plunian, K.-H. Rädler. Harmonic and subharmonic solutions of the Roberts dynamo problem. Application to the Karlsruhe experiment *Magnetohydodynamics*, vol. 38 (2002), no. 1-2, pp. 95–106.

[7] Yu.B. Ponomarenko. On the theory of the hydromagnetic dynamo. *J. Applied Mech. Tech. Phys.*, vol. 14 (1973), pp. 775.

[8] A. Gailitis, O. Lielausis, E. Platacis, S. Dement'ev, A. Cifersons, G. Gerbeth, Th. Gundrum, F. Stefani, M. Christen, G. Will. Dynamo experiments at the Riga sodium facility *Magnetohydodynamics*, vol. 38 (2002), no. 1-2, pp. 5–14.
A. Gailitis, O. Lielausis, E. Platacis,G. Gerbeth, F. Stefani. On back-reaction effects in the Riga dynamo experiment. *Magnetohydodynamics*, vol. 38 (2002), no. 1-2, pp. 15–26.

[9] N.L. Dudley, R.W. James. Time-dependent kinematic dynamos with stationary flows. *Proc. Roy. Soc. Lond.*, vol. A425, (1989), pp. 407.

[10] L. Marié et al. Numerical study of homogeneous dynamo based on experimental von Kármán flows. *Eur. J. Phys. B*, vol. 33 (2002), pp. 469–485.

[11] Dynamo and Dynamics, A Mathematical Challenge. Proceedings of the NATO Advanced Research Workshop, Cargèse (France), August 21-26, 2000. NATO Science series II, Vol. 26, P. Chossat, D. Armbruster and I. Oprea eds. Kluwer Academic Publishers, Dordrecht, The Netherlands (2001).

[12] P. Odier, J.-F. Pinton, S. Fauve. Advection of a magnetic field by a turbulent swirling flow. *Phys. Rev. E*, vol. 58, (1999), pp. 7397.

[13] P. Odier, J.-F. Pinton, S. Fauve. Magnetic induction by coherent vortex motion. *Eur. Phys. J. B*, vol. 16, (2000), pp. 373.

[14] F. Krause, K.-H. Rädler. *Mean-Field Electrodynamics and Dynamo Theory* (Oxford, Pergamon, 1980).

[15] A. Lanotte et al. A large scale dynamo by negative eddy diffusivity. *Geophys. Astrophys. Fluid Dyn.*, vol. 91, (1999), pp. 131.

[16] E.N. Parker. Hydromagnetic dynamo models. *Astrophysical J.*, vol. 122, (1955), pp. 293-314.

[17] F. Pétrélis et al. Non linear magnetic induction by helical motion in a liquid sodium turbulent flow. *Phys. Rev. Lett.*, vol. 90 (2003), p. 174501.

[18] N.L. Peffley, A.B. Cawthrone, D.P. Lathrop. Toward a self-generating magnetic dynamo: the role of turbulence. *Phys. Rev. E*, vol. 61, (2000), pp. 5287.

[19] M. Bourgoin et al., MHD measurements in the von Kármán sodium experiment. *Phys. Fluids*, vol. 14, (2002), pp. 3046.

[20] F. Ravelet, A. Chiffaudel, F. Daviaud. private communication.

[21] D. Brito, P. Cardin, H.-C. Nataf, G. Marolleau. Experimental study of a geostrophic vortex of Gallium in a transverse magnetic field. *Phys. Earth Planet. Int.*, vol. 91, (1995), pp. 77–98.

[22] A. Brisseau, U. Frisch, J. Lérorat, M., Lessieur, A. Mazure. Helicity cascade in fully developed turbulence. *Phys. Fluids*, vol. 16, (1973), pp. 1366.

[23] Q. Chen, S. Chen, G.L. Eyink. The joint cascade of energy and helicity in three dimensional turbulence. *Phys. Fluids.*, vol. 15, (2003), pp. 361.

[24] L. Marié, F. Pétrélis, M. Bourgoin, J. Burguete, A. Chiffaudel, F. Daviaud, S. Fauve, P. Odier, J.-F. Pinton. Open questions about homogeneous fluid dynamos: the VKS experiment. *Magnetohydodynamics*, vol. 38 (2002), no. 1-2, pp. 163–176.

[25] D. Franck, Stacey et al. Electronic and thermal conductivity of the Earth core. *Phys. Earth Plan. Int.*, vol. 124, (2001), pp. 153–162.

Received 09.04.2003